A Photoaffinity Analogue of Discodermolide Specifically Labels a Peptide in β-Tubulin†

Shujun Xia,‡ Craig S. Kenesky,§ Paul V. Rucker,§ Amos B. Smith, III,§ George A. Orr,‡ and Susan Band Horwitz*,‡

Department of Molecular Pharmacology, Albert Einstein College of Medicine, Bronx, New York 10461, and Department of Chemistry, University of Pennsylvania, Philadelphia, Pennsylvania 19104

Received March 13, 2006; Revised Manuscript Received June 9, 2006

ABSTRACT: Discodermolide is a potentially important antitumor agent that stabilizes microtubules and blocks cells at the G2/M phase of the cell cycle in a manner similar to that of Taxol. Discodermolide also has unique properties that distinguish it from Taxol. In the present study, photoaffinity-labeled discodermolide analogues are used to investigate their binding site in tubulin. Three photoaffinity-labeled discodermolide analogues were synthesized, all of which promoted microtubule polymerization in the absence of GTP. The analogue, C19-[4-(4-^{3}H-benzoyl-phenyl)-carbamate]-discodermolide (C19-[^{3}H]BPC-discodermolide), was selected for photolabeling studies because it had the highest extent of photoincorporation, ∼1%, of the three radiolabeled discodermolide analogues explored. Although compared to discodermolide, C19-BPC-discodermolide revealed no hypernucleation effect in the *in vitro* microtubule polymerization assay, it was more cytotoxic than discodermolide, and, like discodermolide, demonstrated synergism with Taxol. These results suggest that the hypernucleation effect of discodermolide is not involved in its cytotoxic activity. Similar to discodermolide, C19-BPC-discodermolide can effectively displace [^{3}H]Taxol from microtubules, but Taxol cannot effectively displace C19-[^{3}H]BPC-discodermolide binding. Discodermolide can effectively displace C19-[^{3}H]BPC-discodermolide binding. Formic acid hydrolysis, immunoprecipitation experiments, and subtilisin digestion indicate that C19-BPC-discodermolide labels amino acid residues 305−433 in β-tubulin. Further digestion with Asp-N and Arg-C enzymes suggested that C19-BPC-discodermolide binds to amino acid residues, 355−359, in β-tubulin, which is in close proximity to the Taxol binding site. Molecular modeling guided by the above evidence led to a putative binding model for C19-BPC-discodermolide in tubulin.

Taxol, an antitumor agent used successfully in the treatment of breast, ovarian, and lung carcinomas (*1*), targets the β-tubulin subunit of the microtubule. Taxol can promote microtubule polymerization in the absence of GTP, which is normally required for microtubule polymerization, and the microtubules formed are stable to cold- and calcium-induced depolymerization (*2*). Previously, our laboratory employed three photoaffinity-labeled Taxol analogues to identify the Taxol binding site in β-tubulin (*3*−*5*). More recently, with the development of a high-resolution structure of the αβ-tubulin dimer (*6*), several Taxol binding conformations have been proposed (*7*−*9*).

The low aqueous solubility of Taxol that has made the drug difficult to administer, in conjunction with the development of Taxol resistance in patients (*10*), has led to the search for new compounds with a mechanism similar to that of Taxol, but with enhanced therapeutic activity. This effort has led to the discovery of a number of molecules including epothilones, eleutherobin, discodermolide, laulimalide, peloruside A, ceratamines, and dictyostatin (*11*−*17*). Downing and co-workers reported that epothilone A has an overlapping binding site with Taxol on β-tubulin (*18*). Results of a computational search proposed that laulimalide and peloruside A bind to α-tubulin (*19*). Discodermolide is an especially interesting molecule that has Taxol-like microtubule stabilizing properties but also has characteristics that are distinct from Taxol. In addition, discodermolide is a considerably weaker substrate for P-glycoprotein than Taxol (*12*).

Discodermolide was first reported as a potential immunosuppressive agent (*20*, *21*), but was later found to act like Taxol in promoting microtubule polymerization and suppressing microtubule dynamic instability (*22*). However, studies also indicated that there are definite differences between discodermolide and Taxol. In the *in vitro* microtubule polymerization assay, discodermolide demonstrates a very strong hypernucleation effect when initiating microtubule assembly. Short microtubule polymers were formed compared to the long microtubules found with Taxol (*12*). Discodermolide can competitively inhibit [^{3}H]Taxol binding to microtubules, but surprisingly, cell lines with β-tubulin mutations that make them resistant to Taxol are not cross-resistant to discodermolide (*23*, *24*). Unlike the other microtubule-stabilizing drugs such as the epothilones and eleutherobin, discodermolide does not substitute very well for Taxol in A549-AT12 cells, which are, in addition to being

* To whom correspondence should be addressed. Phone: (718) 430-2163. Fax: (718) 430-8959. E-mail: shorwitz@aecom.yu.edu.

† This work was supported by U.S. Public Health Service, National Cancer Institute, CA083185 and CA077263; National Foundation for Cancer Research (S.B.H.); and NIH Institute of General Medical Sciences, GM29028 (A.B.S.).

‡ Albert Einstein College of Medicine.

§ University of Pennsylvania.

10.1021/bi060497a CCC: $33.50
Published on Web 09/09/2006

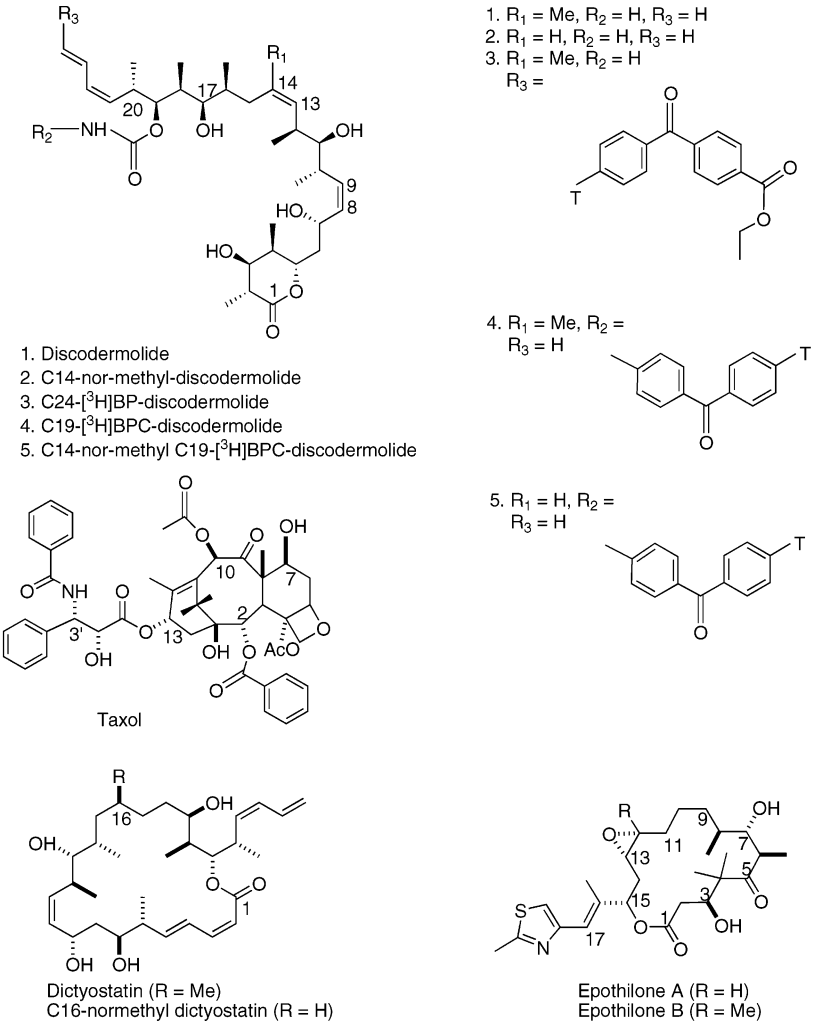

FIGURE 1: Chemical structures of discodermolide, discodermolide analogues, dictyostatin, Taxol, and epothilones. (1) Discodermolide; (2) C14-nor-methyl-discodermolide; (3) C24-[^{3}H]BP-discodermolide; (4) C19-[^{3}H]BPC-discodermolide; (5) C14-nor-methyl C19-[^{3}H]BPC-discodermolide. T = tritium.

resistant to Taxol, dependent on low levels of Taxol for normal cell growth (*25*). A most interesting observation, however, is that discodermolide can induce accelerated cell senescence, which is not a typical characteristic of Taxol (*26*).

Our laboratories recently investigated the efficacy of discodermolide and Taxol combinations, demonstrating synergism both in cell culture and in an ovarian xenograft tumor model in nude mice (*25*, *27*). Discodermolide and Taxol both suppress microtubule dynamics, but discodermolide barely interferes with length-based catastrophe frequency, which is significantly increased upon Taxol treatment (*22*). Discodermolide and Taxol can synergistically suppress microtubule dynamic instability (*28*). The distinct effects of discodermolide and Taxol on microtubules may result from either different binding sites in the $\alpha\beta$-tubulin dimer, specific interactions with individual tubulin isotypes, or different affinities for $\alpha\beta$-tubulin dimers located at distinct regions of the microtubule. Definition of the discodermolide binding site(s) in the microtubule and comparison to that of the Taxol binding site could provide us with new insights into the synergism observed between the two drugs.

Previously, our laboratories modeled two possible discodermolide docking conformations in the drug binding pocket in tubulin (*29*). In the present study, we further investigated this pocket. Since structure−activity relationship (SAR) studies indicated that the C19 carbamate moiety and C24 diene system are relatively tolerant to modifications (*30*−*32*), photoreactive groups were placed at these positions. We tested three photoaffinity-labeled discodermolide analogues (Figure 1). One analogue, C19-[4-(4-^{3}H-benzoyl-phenyl)-carbamate]-discodermolide (C19-[^{3}H]BPC-discodermolide),[1] was selected to investigate the discodermolide binding site in the microtubule. Our results indicate the C19 carbamate group of C19-[^{3}H]BPC-discodermolide binds to a sequence containing amino acid residues 305−433, specifically, 355−359 in the S9−S10 loop in β-tubulin. This led to the molecular modeling of the conformation of the discodermolide analogue and discodermolide in β-tubulin.

MATERIALS AND METHODS

Materials. Microtubule protein (MTP) was purified from calf brain by two cycles of temperature-dependent assembly

[1] Abbreviations: BP, benzophenone; BPC, benzophenone carbamate; CI, combination index; DMSO, dimethyl sulfoxide; HPLC, high-performance liquid chromatography; MES, 2-(*N*-morpholino) ethanesulfonic acid; MTP, microtubule protein; PAGE, polyacrylamide gel electrophoresis; PMSF, phenylmethanesulfonyl fluoride; TFA, trifluoroacetic acid.

disassembly and stored in 0.1 M MES, 1 mM EGTA, 0.5 mM $MgCl_2$, and 3 M glycerol, pH 6.6, in liquid nitrogen. The concentration of tubulin in MTP was based on a tubulin content of 85% (*3*). Before each experiment, centrifugation (55 000 rpm, 20 min, 4 °C, TLA 100.3 rotor, Optima TLX Ultracentrifuge, Beckman Coulter) was done to remove protein aggregates. The discodermolide analogues (Figure 1) were C24-[^{3}H]benzoyl-phenyl-discodermolide (C24-[^{3}H]-BP-discodermolide, 5.2 Ci/mmol), C19-[^{3}H][4-(4-benzoyl-phenyl)-carbamate]-discodermolide (C19-[^{3}H]BPC-discodermolide, 4.1 Ci/mmol), and C14-nor-methyl C19-[^{3}H][4-(4-benzoyl-phenyl)-carbamate]-discodermolide (C14-nor-methyl C19-[^{3}H]BPC-discodermolide, 4.3 Ci/mmol). The syntheses have been reported previously (*33*). Taxol and [^{3}H]-Taxol (19.3 Ci/mmol) were obtained from the Drug Development Branch, National Cancer Institute, Bethesda, MD. Drugs were dissolved in dimethyl sulfoxide (DMSO) to a final concentration of 5 mM, except that in one of the *in vitro* microtubule polymerization assays, drugs were dissolved in DMSO/Tween = 1:1 (v/v) to increase solubility. GTP was dissolved in dH_2O. Tricine, formic acid, acetone, subtilisin, iodoacetamide, and acetonitrile were purchased from Sigma. Trifluoroacetic acid and guanidine hydrochloride were from Pierce. EN^{3}HANCE was obtained from DuPont NEN. Asp-N and Arg-C enzymes were from Roche. The non-small cell human lung cancer cell line A549 was maintained in RPMI 1640 containing 1% penicillin−streptomycin (Gibco Laboratories, Grand Island, NY) and 10% fetal bovine serum. Tween was purchased from Bio-Rad.

In vitro Microtubule Polymerization Assay. Drugs were dissolved in either DMSO/Tween (v/v = 1:1) or DMSO. Assays were done in a 300 μL quartz cuvette. Drugs (10 μM) or GTP (1 mM) was added to 1 mg/mL MTP. Assembly of microtubule protein was monitored spectrophotometrically (Application of MltiTemp, Beckman Coulter DU640) by recording changes in turbidity at 350 nm at 37 °C. After 60 min, the temperature was decreased to 2 °C to determine the effect of cold on stabilization of microtubules by the analogues.

Electron Micrographs of Microtubules. At the end of the microtubule polymerization assay, samples were put onto 300-mesh carbon-coated, Formavar-treated copper grids, stained with 2% uranyl acetate, and viewed with a JEOL model 100CX electron microscope. On samples polymerized with drug dissolved in DMSO/Tween, microtubule lengths were measured at 2000× and 5000× with ImageJ software and compared. Fifty microtubules were counted for each sample, except for C14-nor-methyl C19-BPC-discodermolide where only 30 microtubules were counted because so few microtubules were formed.

Cytotoxicity Assay and Drug Combination Analysis. Cytotoxicity assays and drug combination analyses were performed as described previously (*25*). Briefly, the individual drug or drug combinations, at different ratios, were added to the cells, and after incubation for 72 h, the CellTiter 96 Aqueous non-radioactive cell proliferation assay was used to determine the number of live cells. IC_{50} values were calculated with Calcusyn software. The individual IC_{50} value was used as the equipotent drug concentration in drug combination assays. In addition, Taxol and C19-BPC-discodermolide were tested at ratios of 1:14, 1:3.5, 1:1, 3.5:1, and 14:1. C19-BPC-discodermolide and discodermolide were tested at ratios of 1:7, 1:2, and 1:1. The combination index (CI) method of Chou and Talalay (*25*) was used to analyze the interactions between Taxol, epothilone B, discodermolide, and C19-BPC-discodermolide. Data represent mean CI values from three experiments.

Photoaffinity Labeling of Tubulin. Photoaffinity labeling was done as described previously (*5*). Tubulin (2 μM) was polymerized into microtubules in the presence of 0.2 mM GTP and either 2 μM C24-[^{3}H]BP-discodermolide, C19-[^{3}H]-BPC-discodermolide, or C14-nor-methyl C19-[^{3}H]BPC-discodermolide plus 20-fold excess of cold competitor for 30 min at 37 °C. Samples were irradiated for 2 h on ice water using a 350 nm ultraviolet light (model RPR-3500 Å; Southern New England Ultraviolet Co., Branford, CT) at a distance of 1.5 cm. After UV irradiation, samples were centrifuged in a Ti42.2 rotor in a Beckman L7 ultracentrifuge at 100 000*g* for 30 min at 27 °C to precipitate assembled microtubules. The protein pellets were resolved by 9% sodium dodecyl sulfate−polyacrylamide gel electrophoresis (SDS−PAGE) to separate $\alpha\beta$-tubulin subunits. Western blots were done to identify α and β tubulin subunits. For fluorography, the gel was stained with Coomassie Blue R-250, destained, treated with EN^{3}HANCE, dried, and exposed to Kodak X-Omat AR film at −70 °C for 7 days.

Competiton Studies. Experiments were done as described previously (*34*, *35*). Briefly, 200 μL of 2 μM tubulin was polymerized in the presence of 0.2 mM GTP and different cold microtubule interacting drugs. After incubation for 20 min at 37 °C, 2 μM C19-[^{3}H]BPC-discodermolide or [^{3}H]Taxol was added for another 2 h, and the samples were layered onto 20 μL of 5% sucrose in 0.1 M MES tubulin assembly buffer containing 3 M glycerol and centrifuged in a Ti42.2 rotor in a Beckman L7 ultracentrifuge at 100 000*g* for 1 h at 27 °C. After centrifugation, the supernatant was carefully removed, and the pellet was washed three times with 0.1 M MES buffer and dissolved in 10 mM sodium phosphate buffer containing 1% SDS. Radioactivity was determined in a liquid scintillation counter (Perkin-Elmer). Protein concentration was measured by the DC Protein Assay from Bio-Rad Laboratories. After correcting for a small amount of nonspecifically sedimented protein, we calculated the ratio between tubulin dimer and C19-[^{3}H]BPC-discodermolide. Drug competition was also analyzed by fluorography. C19-[^{3}H]BPC-discodermolide or [^{3}H]Taxol was added after incubation of tubulin with different microtubule interacting drugs (at 50-fold excess). After UV irradiation (350 nm for 2 h for C19-[^{3}H]BPC-discodermolide and 254 nm for 30 min for [^{3}H]Taxol), samples were resolved by SDS−PAGE on a 9% gel followed by fluorography (7 days for C19-[^{3}H]BPC-discodermolide and 40 days for [^{3}H]Taxol).

Formic Acid Digestion. Tubulin was photolabeled with C19-[^{3}H]BPC-discodermolide and digested with 75% formic acid for 96 h at 37 °C (*3*). After removal of formic acid by Speedvac and washing three times with dH_2O, digestion products were resolved on a 15% Tricine gel. Two gels were prepared. One gel was stained with Coomassie blue, and the other gel was visualized by fluorography.

Immunoprecipitation. Immunoprecipitation experiments were done as described previously (*36*, *37*). Briefly, tubulin was photolabeled with C19-[^{3}H]BPC-discodermolide. After formic acid digestion and removal of formic acid by Speedvac, samples were washed three time with dH_2O,

adjusted to pH 7.0, and dissolved in RIPA buffer (20 mM Tris-HCl, pH7.5, 150 mM NaCl, 1% NP40, and 0.1% SDS). Antibodies (anti-α T9026 or anti-β T0198, Sigma) were added and incubated at 4 °C overnight. Protein A-Sepharose CL-4B was used to precipitate immunocomplexes. After washes (five times) with RIPA buffer, samples were resolved on a 15% Tricine gel either for Coomassie blue staining or fluorography.

Subtilisin Digestion. Microtubules were assembled and photolabled by C19-[^{3}H]BPC-discodermolide. Subtilisin was added at a ratio of protein/enzyme = 500:1 (w/w). After digestion for 1 and 12 h, reactions were stopped with 2 mM PMSF. Samples were resolved by SDS−PAGE on a 9% gel followed by fluorography.

Asp-N and Arg-C Enzyme Digeston of β-Tubulin. After tubulin was photolabeled with C19-[^{3}H]BPC-discodermolide, acetone precipitation was performed to remove free unbound drug (1 vol of protein solution plus 4 vol of cold acetone, −20 °C, overnight) (*38*). Samples were then denatured with guanidine hydrochloride, and the cysteine residues were modified by carboxymethylation with iodoacetamide (*4*). α- and β-Tubulin subunits were separated by reverse-phase high-performance liquid chromatography (HPLC) on an Aquapore BU-300 (220 × 2.1 mm) C4 column using HP1090 liquid chromatography. The protein was eluted with a linear acetonitrile, 0.1% trifluoroacetic acid gradient (25%−55% over 60 min). The flow rate was 200 μL/min, and 1 min fractions were collected. The elution of α- and β-tubulin subunits was determined by Western blot. Fractions containing radiolabeled protein were detected with fluorography. Radioactive fractions were collected and dried by Speedvac. Samples were digested with either Asp-N or Arg-C (protein/enzyme = 100:1, w/w) for 6, 12, or 18 h at 37 °C according to the manufacturer's instructions (Roche). The digestion buffer for Asp-N was 50 mM sodium phosphate, pH8.0, containing 1 M urea. Arg-C digestion buffer was 90 mM Tris-HCl, pH7.5, 8.5 mM $CaCl_2$, 5 mM dithiothreitol (DTT), 0.5 mM EDTA, and 1 M urea. Digestion products were resolved on a 10−20% Tricine gel and subjected to fluorography for 30 days.

Molecular Modeling. Calculations were performed on MacroModel 6.5 using the batchmin accessory. C19-BPC-discodermolide was docked into the binding site on β-tubulin presenting the benzophenone moiety in the vicinity of residues 355−359. Loop residues 355−365 were reoriented to enable the benzophenone group to contact the desired sequence. Conformational searches were then executed on a sphere of 10 Å surrounding the binding site allowing flexibility of both the ligand and the site while fixing the benzophenone moiety in contact with residues 355−359 (amino acids were numbered according to a previous publication, ref *10*)

RESULTS

Polymerization of Tubulin by Discodermolide Analogues. The *in vitro* microtubule polymerization assay was used to follow the activity of discodermolide analogues (Figure 2). The change in absorbance at 350 nm correlates with the extent of microtubule polymerization (*39*). Because of the poor solubility of C24-BP-discodermolide and C14-nor-methyl C19-BPC-discodermolide, all drugs were dissolved

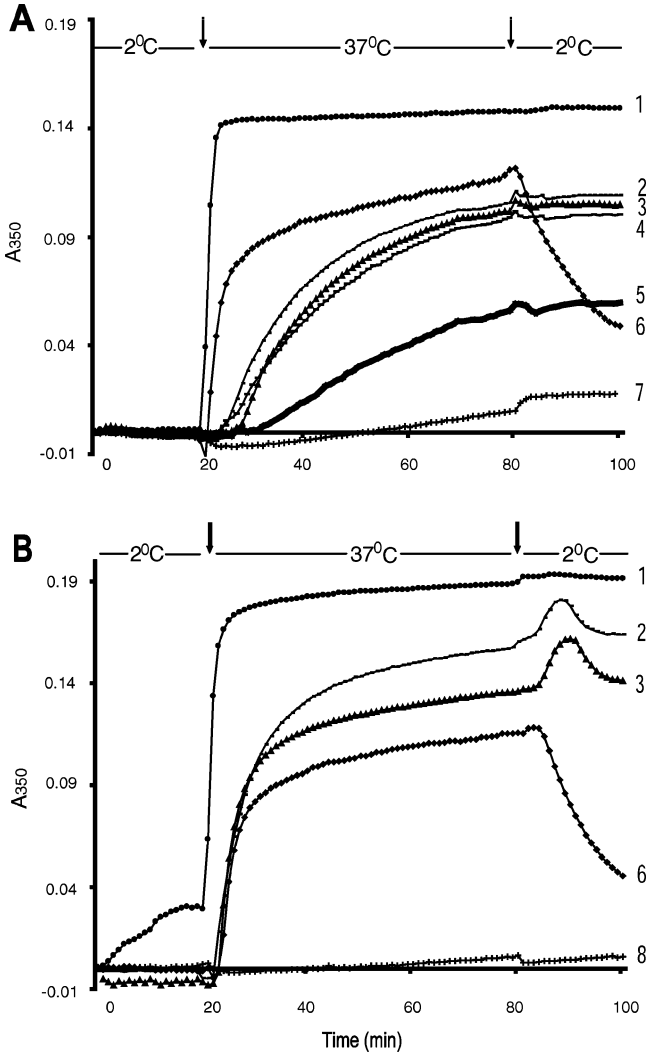

FIGURE 2: *In vitro* microtubule polymerization. Experiments were done as described in Materials and Methods. Drugs were dissolved in either DMSO/Tween (A) or DMSO (B). The arrows (↓) indicate a change in temperature. (1) Discodermolide; (2) Taxol; (3) C19-BPC-discodermolide; (4) C24-BP-discodermolide; (5) C14-nor-methyl C19-BPCdiscodermolide; (6) GTP; (7) DMSO/Tween; (8) DMSO.

in DMSO/Tween (v/v = 1:1). All three discodermolide analogues promoted polymerization of tubulin in the absence of GTP, and the microtubules formed were stable to cold-induced depolymerization (Figure 2A). When Taxol, discodermolide, and C19-BPC-discodermolide were dissolved in DMSO and the assay was repeated, the absorbance of the polymerized microtubules was greater than that when the drugs were dissolved in DMSO/Tween (Figure 2B). The three discodermolide analogues did not display the potent hypernucleation effect seen with discodermolide when polymerization was initiated. C14-nor-methyl C19-BPC-discodermolide was least active. Studies with other discodermolide analogues also revealed that the deletion of the C14 methyl group decreased activity (*29*, *40*, *41*).

Microtubules Formed in the Presence of Discodermolide, Taxol, and Discodermolide Analogues Have Distinct Lengths. To confirm that normal microtubules were being formed, samples were examined by electron microscopy and microtubule lengths were measured (Table 1). Discodermolide produced very short microtubules as has been noted previously (*12*). Taxol, C24-BP-discodermolide, and C19-BPC-

Table 1: A Comparison of Microtubule Lengths after Assembly with Discodermolide, Taxol, Discodermolide Analogues, and GTP

compounds	average polymer length (μm ± SD)
discodermolide	1.05 ± 0.16
Taxol	10.63 ± 1.34
C24-BP-discodermolide	12.62 ± 2.27
C19-BPC-discodermolide	10.60 ± 1.58
C14-nor-methyl C19-BPC-discodermolide	19.70 ± 3.93
GTP	5.46 ± 1.35

Table 2: Cytotoxicity of Taxol, Discodermolide, and Discodermolide Analogues[a]

compounds	IC_{50} ± SD (nM)
discodermolide	19.7 ± 0.2
Taxol	1.4 ± 0.1
C24-BP-discodermolide	18.0 ± 0.9
C19-BPC-discodermolide	7.2 ± 0.2
C14-nor-methyl C19-BPC-discodermolide	40.4 ± 1.6

[a] IC_{50} equals the drug concentration that inhibits cell division by 50% after 72 h.

discodermolide induced long microtubules. C14-nor-methyl C19-BPC-discodermolide produced only a few very long microtubules. The microtubules formed with discodermolide were approximately 10-, 12-, 10-, 19-, and 5-fold shorter than those formed with Taxol, C24-BP-discodermolide, C19-BPC-discodermolide, C14-nor-methyl C19-BPC-discodermolide, and GTP, respectively.

Cytotoxicity of Discodermolide Analogues and Drug Combination Studies. As has been shown previously (*26*, *29*), discodermolide is less toxic to cells than Taxol. Each of the three discodermolide analogues inhibited A549 cell growth to different degrees. C14-nor-methyl C19-BPC-discodermolide was the least active (Table 2). This is consistent with *in vitro* microtubule polymerization results which demonstrated that C14-nor-methyl C19-BPC-discodermolide was least active in inducing microtubule polymerization. The IC_{50} value for C19-BPC-discodermolide was lower than that of discodermolide. The hydrophobic benzophenone group on the analogue may result in a greater accumulation of drugs in cells.

Drug combination analysis confirmed that discodermolide and Taxol represent a synergistic combination in A549 cells,

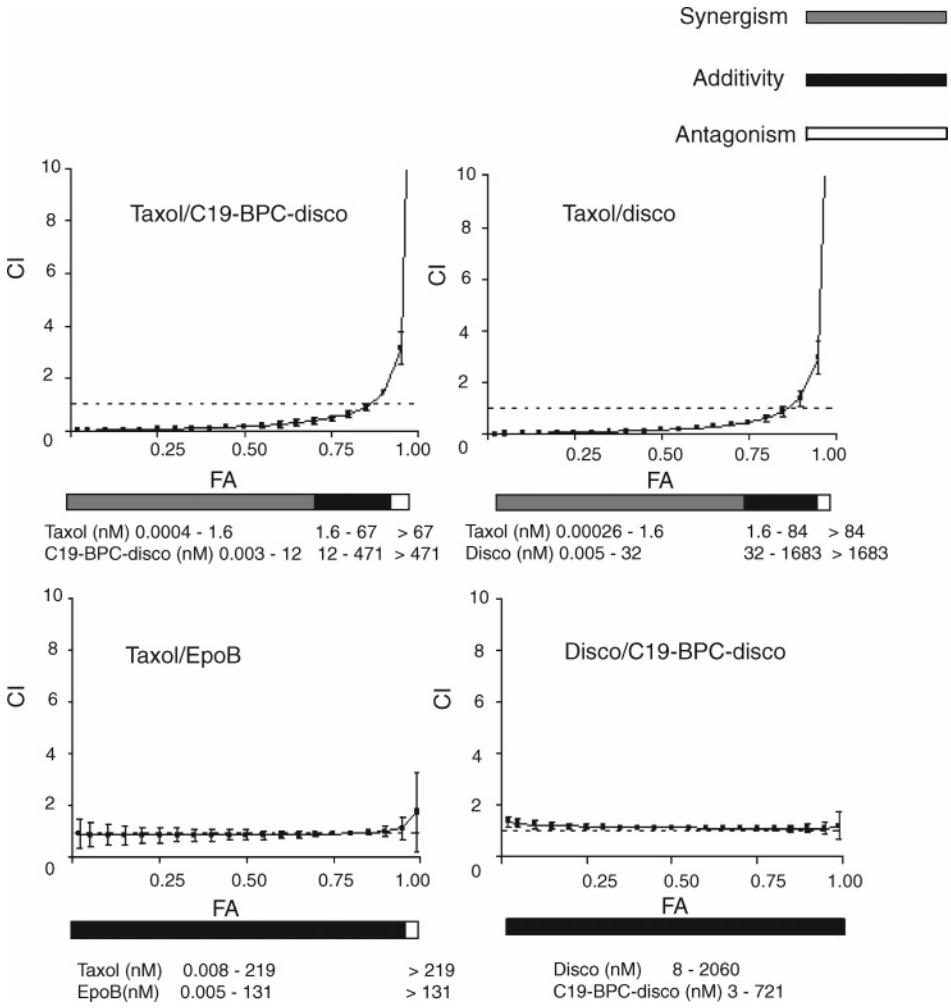

FIGURE 3: C19-BPC-Discodermolide and Taxol represent a synergistic drug combination. Combination index (CI) values as a function of cell kill (fraction affected; FA) were calculated after treating A549 cells with drug combinations for 72 h. Various drug ratios were tested. Data shown here are the results from equipotent molar ratios (Taxol/C19-BPC-discodermolide = 1:7; Taxol/discodermolide = 1:20; Taxol/epothilone B = 1:0.6; discodermolide/C19-BPC-discodermolide = 1:0.35). Data represent mean CI values from three experiments. The dotted line in each graph represents a CI = 1. The gray horizontal bar below the graph indicates the dose range of drugs that show synergistic interactions (CI < 0.7) when in combination. The black horizontal bar corresponds to the CI of 0.7−1.2 and indicates additivity, whereas the white bar corresponds to the CI > 1.2, indicating antagonism. The ranges of drug concentrations that mediate synergism, additivity, or antagonism are indicated.

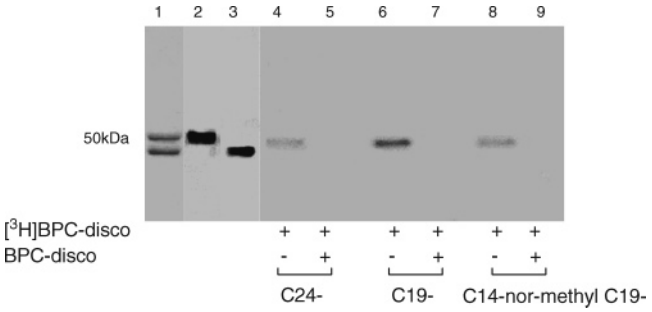

FIGURE 4: Discodermolide analogues specifically photolabel tubulin. Microtubules were polymerized in the presence of C24-[^{3}H]-BP-discodermolide, C19-[^{3}H]BPC-discodermolide, or C14-nor-methyl C19-[^{3}H]BPC-discodermolide plus and minus a 20-fold excess of cold competitor for 30 min. After irradiation with 350 nm UV light, the reaction solutions were resolved by SDS−PAGE and analyzed with either Coomassie staining (lane 1), Western blotting (lane 2, anti-α-tubulin antibody; lane 3, anti-β-tubulin antibody), or fluorography (lanes 4−9). The αβ-tubulin dimer separates by SDS−PAGE under the conditions used (lane 1). Western blotting indicates that the upper band is α-tubulin (lane 2) and the lower band is β-tubulin (lane 3). By fluorography, all three discodermolide analogues can photolabel tubulin (lane 4, 6, and 8), but the photolabeling can be competed by 20-fold excess of cold compounds (lane 5, 7, and 9). C19-BPC-discodermolide demonstrates the highest extent of photoincorporation.

whereas Taxol and epothilone B have an additive effect. At all drug concentrations tested, C19-BPC-discodermolide and Taxol demonstrated a synergistic drug interaction, whereas C19-BPC-discodermolide and discodermolide only demonstrated additivity, but no synergism (Figure 3). These results suggest that C19-BPC-discodermolide has a mechanism of cytotoxicity similar to discodermolide, although it is less potent than discodermolide and has no hypernucleation effect in the *in vitro* microtubule polymerization assay.

Discodermolide Analogues Specifically Label Tubulin. The discodermolide analogues specifically photolabel tubulin since the photolabeling was competed by nontritiated discodermolide analogues (Figure 4). The radioactive band is localized between the α- and β-tubulin subunit. In a previous report, β-tubulin photolabed by a benzophenone Taxol analogue was also located between the α- and β-tubulin subunit when analyzed by SDS−PAGE (*5*). On the basis of a filter binding assay after acetone precipitation, the use of C19-BPC-discodermolide resulted in the greatest extent of photoincorporation, ∼1%. Considering the extent of photoincorporation and solubility, C19-BPC-discodermolide was used in all future experiments. Previous studies have shown that both Taxol and discodermolide have only one binding site on the tubulin dimer (*34*, *42*). The stoichiometry studies with C19-BPC-discodermolide also indicated that it only has one binding site in the αβ-tubulin dimer (data not shown). With the drug concentration increasing, the binding of C19-BPC-discodermolide will saturate. The higher concentration of drug did not cause increased association of the drug to the microtubule. This also confirmed that the binding of C19-BPC-discodermolide to the microtubule is specific.

Competition Analysis with Taxol, Discodermolide, and Discodermolide Analogues. Drug competition analyses were performed to determine if Taxol, discodermolide, and C19-BPC-discodermolide could displace binding of the radiolabled drugs to microtubules. Two methods were employed. One was performed in solution. As shown in Figure 5A, both discodermolide and C19-BPC-discodermolide effectively displaced C19-[^{3}H]BPC-discodermolide binding to the microtubules, but Taxol and epothilone B were not as effective as discodermolide or its analogue. When [^{3}H]Taxol was used, all compounds could effectively displace [^{3}H]Taxol from the microtubules. Competition assays analyzed by fluorography are consistent with the solution competition results (Figure 5B). Taxol cannot effectively displace C19-[^{3}H]BPC-discodermolide, but C19-BPC-discodermolide can effectively displace [^{3}H]Taxol binding to the microtubule. Discodermolide can effectively displace C19-[^{3}H]BPC-discodermolide. It has been previously reported (*42*) that discodermolide can effectively displace [^{3}H]Taxol binding to microtubules, whereas Taxol cannot effectively displace [^{3}H]-discodermolide binding. A possible explanation is that discodermolide and Taxol have different affinities for their microtubule binding sites (*43*) or that they form microtubules with different configurations (*42*). By using previously described methods (*23*), we have shown that, like discodermolide, C19-BPC-discodermolide can competitively inhibit [^{3}H]Taxol binding to microtubules (data not shown). The calculated K_i for discodermolide is 0.25 μM and for C19-BPC-discodermolide is 0.19 μM.

C19-BPC-Discodermolide Binds to the β-Tubulin B3 Fragment. Formic acid is known to cleave Asp-Pro bonds. It has been used to help identify the Taxol binding site in β-tubulin (*3*). α-Tubulin produces two fragments, A1 and A2, when cleaved with formic acid, and β-tubulin is hydrolyzed into three fragments, B1, B2, and B3 (*3*) (Figure 6A). After formic acid digestion and SDS−PAGE, fluorography indicated that the radioactivity was associated primarily with a 16 kDa peptide. It was either the A2 or B3 fragment (Figure 6B). Immunoprecipitation experiments were done to determine which fragment was binding to C19-BPC-discodermolide. After formic acid digestion, samples were immunoprecipitated with either anti-α-tubulin (Figure 6C, lanes 1 and 3) or anti-β-tubulin (Figure 6C, lanes 2 and 4) antibodies, which recognize the C-terminus of either α- or β- tubulin, respectively (*44*, *45*). The C19-[^{3}H]BPC-discodermolide labeled peptide was immunoprecipitated by anti-β antibody but not with anti-α antibody (Figure 6C, lanes 3 and 4). Binding of C19-BPC-discodermolide to the β-tubulin B3 fragment (Figure 6A) was further confirmed because the anti-β-tubulin antibody recognized amino acid residues 427−432 in β-tubulin, which are in the B3 fragment (*45*).

Subtilisin Digestion of Tubulin. Limited proteolysis of tubulin by subtilisin results in significant cleavage at Gln433−Gly434 in β-tubulin. This protease has been used to localize a hemiasterlin analogue binding site in tubulin (*46*). In the Coomassie blue staining gel, β-tubulin has an increased mobility after subtilisin digestion for 1 or 12 h (Figure 6D, lanes 2 and 3), respectively, whereas α-tubulin did not show a significant mobility change. Fluorography indicated that the protein labeled by C19-[^{3}H]BPC-discodermolide had an increased mobility after subtilisin digestion for 1 or 12 h (Figure 6D, lanes 5 and 6), respectively. These results indicated that C19-[^{3}H]BPC-discodermolide binds to β-tubulin. Overlapping the sequences from formic acid and subtilisin digestion indicated that C19-[^{3}H]BPC-discodermolide binds to amino acid residues 305−433 in β-tubulin.

Mapping C19-BPC-Discodermolide Binding Peptide by Asp-N and Arg-C Digestion. To further map the C19-BPC-

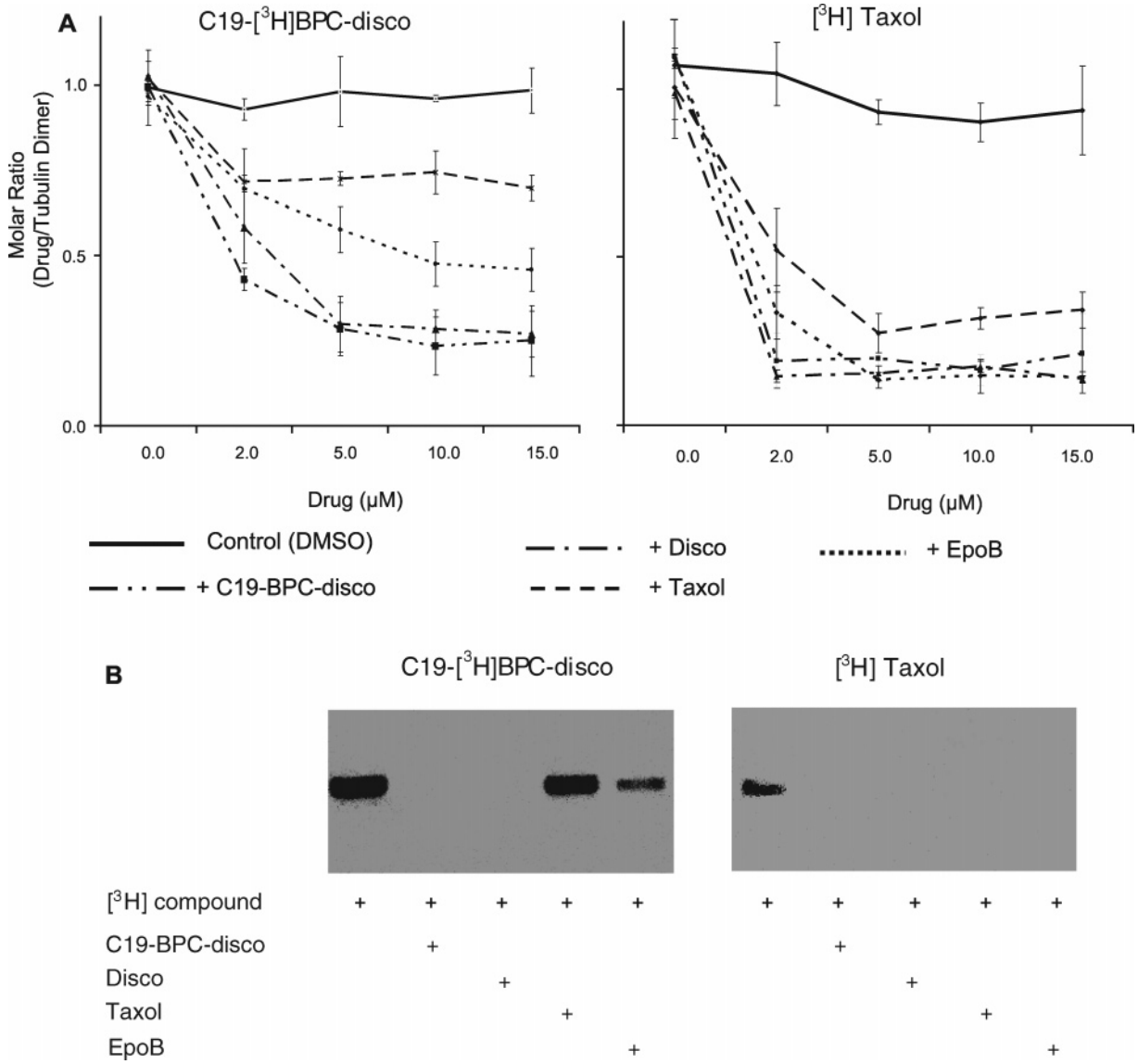

FIGURE 5: Competition assay between Taxol, discodermolide, and C19-BPC-discodermolide. **(**A) Solution competition analyses were performed as described in Materials and Methods. Microtubules were assembled in the presence of different concentrations of each competitor and GTP before the addition of either C19-[^{3}H]BPC-discodermolide or [^{3}H]Taxol. The tritiated drug remaining with the microtubules was determined. After either Taxol or epothilone competition, a significant amount of C19-[^{3}H]BPC-discodermolide remained bound to the microtubules (left panel). Decreased binding of [^{3}H]Taxol to the microtubules was observed after the addition of each of the drugs (right panel). (B) Competitive binding was also analyzed by fluorography. C19-[^{3}H]BPC-discodermolide or [^{3}H]Taxol (2 μM) was added after incubating tubulin with different competitors (100 μM) and GTP. In the left panel, either Taxol or epothilone B could not significantly compete C19-[^{3}H]BPC-discodermolide binding to the microtubule. In the right panel, all competitors could displace [^{3}H]Taxol binding to the microtubule.

discodermolide binding site in β-tubulin, we used Asp-N and Arg-C to digest β-tubulin. After tubulin was photolabeled with C19-[^{3}H]BPC-discodermolide, acetone precipitation was done to remove free unbound drug, so it would not mix with small peptides at the bottom of the gel. After reduction/alkylation, the samples were analyzed by HPLC. Under the chromatography conditions used, α- and β-tubulin were separated and detected with specific antibodies. β-Tubulin eluted first; the major radioactive peak was associated with these fractions (data not shown). The radioactive fractions were collected, dried, and digested with either the Asp-N or Arg-C enzyme for 6, 12, or 18 h, and the digestion products were resolved on a 10−20% Tricine gel. The products were exposed for fluorography for 30 days. All three time points produced the same results. In the Asp-N digestion, the radioactive labeled peptide has a molecular weight of ∼6 kDa (Figure 7A). Arg-C digestion produced a radioactive labeled peptide with a molecular weight of ∼4.5 kDa (Figure 7A). However, due to the low extent of photoincorporation and low specific activity of C19-[^{3}H]BPC-discodermolide, we were not able to isolate and sequence these peptides. Therefore, we compared our present results with protein data bank search outcomes (ProteinProspector) (Figure 7B). Formic acid hydrolysis, immunoprecipitation, and subtilisin digestion suggested that the amino acid residues 305−433 in β-tubulin are the fragment for the binding of C19-BPC-discodermolide (Figure 6). The database search outcomes for this fragment in the β-tubulin digested with either Asp-N or Arg-C are listed in Figure 7B. Because there is only one specific photolabeling site for C19-BPC-discodermolide per $\alpha\beta$-tubulin subunit, the potential drug-labeled peptides digested from either Asp-N or Arg-C should overlap. When

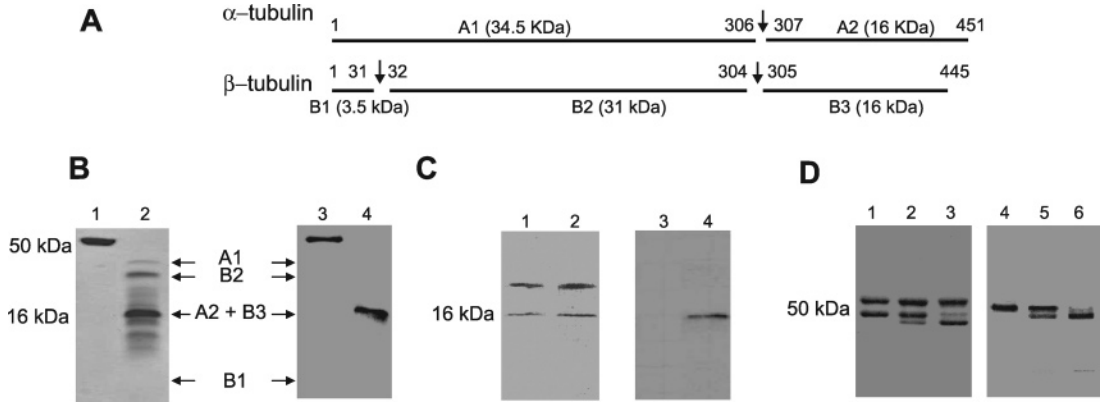

FIGURE 6: C19-[^{3}H]BPC-discodermolide photolables β-tubulin. (A) Schematic representation of formic acid cleavage of α- and β-tubulins. (B) Undigested (lanes 1 and 3) and formic acid-digested (lanes 2 and 4) tubulins were resolved on a 15% Tricine gel and analyzed by either Coomassie blue staining (lanes 1 and 2) or fluorography (lanes 3 and 4). C19-[^{3}H]BPC-discodermolide labels a peptide with a molecular weight of 16 kDa (lane 4). (C) Formic acid digestion products of tubulin were immunoprecipitated with either anti-α- (lanes 1 and 3) or anti-β-tubulin (lanes 2 and 4) antibodies and followed by either Coomassie blue staining (lanes 1 and 2) or fluorography (lanes 3 and 4). C19-[^{3}H]BPC-discodermolide photolabels a peptide which was immunoprecipitated with anti-β-tubulin antibody (lane 4). (D) Limited subtilisin digestion results in significant cleavage at Gln433−Gly434 in β-tubulin. Undigested (lanes 1 and 4) and subtilisin-digested (lanes 2 and 5, 1 h digestion; lane 3 and 6, 12 h digestion) tubulins were resolved on a 9% SDS−PAGE and analyzed with either Coomassie blue staining (lanes 1−3) or fluorography (lanes 4−6). At 1 and 12 h, β-tubulin was digested by subtilisin but α-tubulin was left intact (lanes 2 and 3). C19-[^{3}H]BPC-discodermolide labels β-tubulin since the radiolabeled tubulin was digested by subtilisin at 1 and 12 h (lanes 5 and 6). The photolabeled peptide is amino acid residues 1−433 in β-tubulin.

the molecular weight for each peptide and all the possible peptide combinations are compared, there is only one single possibility for drug labeling. The peptides likely to be labeled by C19-[^{3}H]BPC-discodermolide are marked (■) in Figure 7B. Their molecular weights are 5.7 and 4.6 kDa, respectively, for Asp-N and Arg-C digestions. These are compatible with the experimental results (Figure 7A). The overlapping sequence for these two peptides is amino acid residues 355−359, which is located in the S9−S10 loop. Therefore, the C19 carbamate benzophenone of C19-BPC-discodermolide binds to amino acid sequence 305−433, specifically, to the amino acid residues 355−359 in the S9−S10 loop in β-tubulin (Figure 7C). This led to the molecular modeling of C19-BPC-discodermolide binding conformation in the β-tubulin.

Molecular Modeling of C19-BPC-Discodermolide in β-Tubulin. Identification of the residues which cross-link C19-BPC-discodermolide has allowed the construction of a feasible model for C19-BPC-discodermolide docking into β-tubulin, employing the cocrystal structure of Taxol and tubulin (*47*). The Taxol/tubulin complex is illustrated in Figure 8A with Taxol in red. If C19-BPC-discodermolide were to bind at this site in such a way that the ligand presents the benzophenone moiety to amino acids 355−359, then a conformational change within the binding site would be expected (Figure 8B).

Reorientation of the S9−S10 loop as depicted in Figure 8B reveals a new subpocket within the binding site, not apparent in the cocrystal structure, which incorporates a wall comprised of residues 355−359. The resultant conformation is stabilized by a salt-bridge not observed in the cocrystal structure of Taxol bound to β-tubulin. Figure 8A reveals that the distance between loop residue Lys362 (blue) and Glu325 (red), a residue not associated with the site, is 8.015 Å. Figure 8B illustrates that, in the alternative loop conformation, this distance contracts to 2.608 Å, which suggests a putative salt bridge between these two amino acids. Glu325 is in the H10 helix, which participates in the lateral interaction between adjacent protofilaments (*6*).

Docking calculations of C19-BPC-discodermolide into the modified Taxol site furnish the binding motif depicted in Figure 8B. C19-BPC-discodermolide is illustrated in orange. The benzophenone moiety extends into the new subsite and contacts amino acid residues 355−359 in the S9−S10 loop, a relationship that could not have been achieved without the conformational change of the loop. Reorganization of the drug binding pocket was also observed by electron crystallography in the binding of epothilone A to β-tubulin (*18*).

We also compared the conformations between Taxol and C19-BPC-discodermolide (Figures 9A,C). The C19-benzophenone carbamate of C19-BPC-discodermolide, which corresponds to the C2′ hydroxyl of Taxol, is pointing toward the S9−S10 loop. The δ-lactone of C19-BPC-discodermolide overlaps with the C2 benzoyl of Taxol, and both groups are close to Asp224. The C11 hydroxyl group of C19-BPC-discodermolide matches the C7 hydroxyl group of Taxol, making contact with Thr274. This is similar to the epothilone A binding model in β-tubulin, in which the C7 hydroxyl of epothilone A also participates in the interaction with Thr274 (*18*). In the C19-BPC-discodermolide binding model, Gly360 has been pushed upward because of the conformational change of the S9−S10 loop. The C14 methyl group of C19-BPC-discodermolide interacts with Phe270 in a manner similar to the C4 acetate of Taxol (Figure 9C).

DISCUSSION

Our studies have focused on three discodermolide analogues: C19-BPC-discodermolide, C14-nor-methyl C19-BPC-discodermolide, and C24-BPC-discodermolide. Although all three have lost the hypernucleation effect seen with discodermolide, they all promote, with varying efficiency, microtubule polymerization. In the cytotoxicity assays, all three discodermolide analogues inhibited cell growth. The nor-methyl analogue, C14-nor-methyl C19-

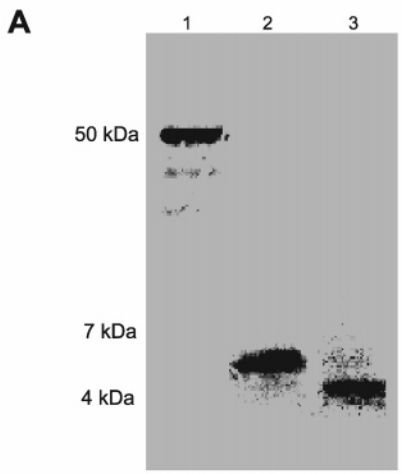

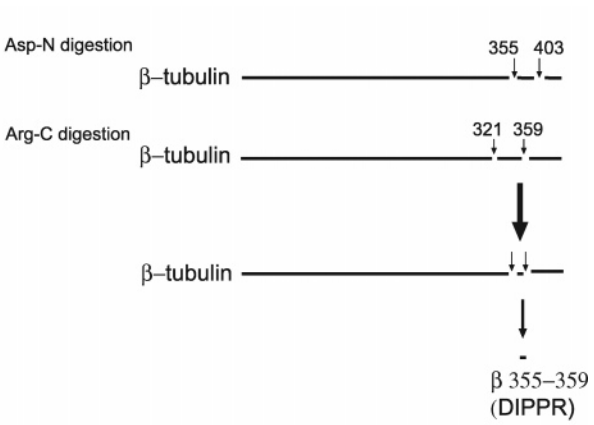

B Asp-N digestion

Calculated peptide mass (Da)	Pepetide sequence
377.4	427DATA430
1273.4	417DLVSEYQQYQ426
1427.4	431DEQGEFEEEGEE442
1547.6	404DEMEFTEAESNMN416
2678.2	304DPRHGRYLTVAAVFRGRMSMKEV326
3330.7	327DEQMLNVQNKNSSYFVEWIPNNVKTAVC354
■5681.7	355DIPPRGLKMSATFIGNSTAIQELFKRISEQFTAMFRRKAFLHWYTG EGM403

Arg-C digestion

Calculated peptide mass (Da)	Pepetide sequence
232.3	319GR320
369.4	307HGR309
1040.3	310YLTVAAVFR318
1230.4	381ISEQFTAMFR390
2313.7	360GLKMSATFIGNSTAIQELFKR380
2741.2	283ALTVPELTQQMFDAKNMMAACDPR306
■ 4615.3	321MSMKEVDEQMLNVQNKNSSYFVEWIPNNVKTAVCDIPPR359
6305.6	392KAFLHWYTGEGMDEMEFTEAESNMNDLVSEYQQYQDATADE QGEFEEEGEEDEA445

FIGURE 7: Asp-N and Arg-C digestion mapping of C19-[^{3}H]BPC-discodermolide photolabled β-tubulin. (A) Tubulin was photolabled by C19-[^{3}H]BPC-discodermolide as described in Materials and Methods. After separating α- and β-tubulin subunits by HPLC, the major radioactive fractions were collected and digested with either Asp-N or Arg-C for 6, 12, or 18 h at 37 °C. The data shown represents a 6 h digestion. All three digestion time points gave the same results. The undigested (lane 1) and digested tubulin products (lane 2, Asp-N digestion; lane 3, Arg-C digestion) were resolved on a 10−20% Tricine gel, followed by fluorography. In Asp-N digestion, C19-[^{3}H]BPC-discodermolide photolabels a peptide with a molecular weight of ~6 kDa. In Arg-C digestion, C19-[^{3}H]BPC-discodermolide photolables a peptide with a molecular weight of ~4.5 kDa. (B) Predicted digestion products from Asp-N and Arg-C digestion of the β-tubulin (Proteinprospector). Since formic acid hydrolysis, immunoprecipitation, and subtilisin digestion results demonstrated that β-tubulin 305−433 is the binding site for C19-[^{3}H]BPC-discodermolide, the peptides listed are 304−442 for Asp-N digestion and 283−445 for Arg-C digestion. The peptide which is most likely to bind to C19-[^{3}H]BPC-discodermolide is noted (■). (C) Schematic representation of overlapping sequences from Asp-N and Arg-C digestion. C19-[^{3}H]BPC-discodermolide is proposed to bind to amino acids 355−359 in β-tubulin.

BPC-discodermolide, was the least active of the three analogues. These results are in accord with previous studies (*29*−*32*).

Formic acid hydrolysis, immunoprecipitation experiments, and subtilisin digestion revealed the cross-linking of the drug to the 305−433 sequence of β-tubulin. Further digestion with Asp-N and Arg-C led to the identification of the 355−359 sequence as the potential site of cross-linking with C19-BPC-discodermolide. This five amino acid sequence is located in the S9−S10 loop, and is a component of the Taxol binding pocket (*6*). In the T-Taxol binding motif, the C2′ hydroxyl group of Taxol forms a hydrogen bond with the carbonyl oxygen of Arg359 (Figure 8A) (*47*), which is in the S9−S10 loop. This is compatible with our results indicating that C19-BPC-discodermolide can displace [^{3}H]Taxol binding to the microtubule and Taxol can partially decrease C19-[^{3}H]BPC-discodermolide binding to the microtubule. With the identification of these five amino acid residues, we have constructed a binding model for C19-BPC-discodermolide in β-tubulin (Figure 8B).

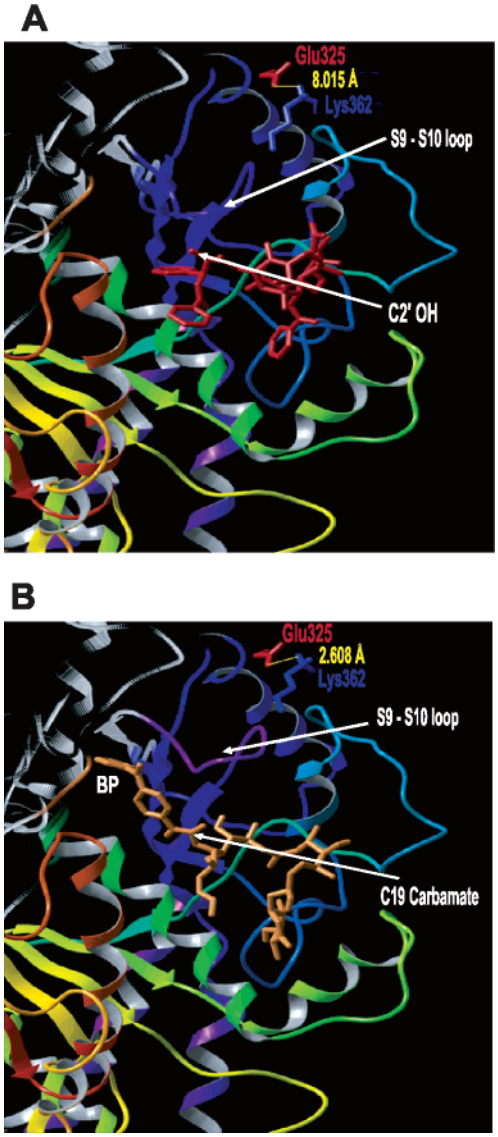

FIGURE 8: Docking of Taxol and C19-BPC-discodermolide into the drug binding pocket in β-tubulin. (A) A cocrystal structure of Taxol and tubulin as determined by Nogales (PDB file 1JFF). Taxol (red) is in the T-conformation. C2′-hydroxyl group of Taxol points toward the S9−S10 loop (purple). The distance between Lys362 (blue) and Glu325 (red) is 8.015 Å. (B) C19-BPC-discodermolide (orange) docked into the β-tubulin. The S9−S10 loop has been modified to enable the ligand to achieve direct contact with amino acid residues 355−359. The C19-carbamate is close to the S9−S10 loop (purple). The distance between Lys362 (blue) and Glu325 (red) is 2.608 Å. (BP = benzophenone).

Discodermolide displays a unique hypernucleation effect when initiating *in vitro* microtubule polymerization (*12*). We found that C19-BPC-discodermolide could promote microtubule polymerization but had lost its hypernucleation effect. This result was expected since other discodermolide analogues, even those with a single change in their chemical structure, lose the hypernucleation effect (*29*, *49*). As suggested by the studies from Kowalski (*23*, *50*), the length of microtubules is related to the nucleation ability and the polymerization activity of the drug. Thereby, it is not surprising that C19-BPC-discodermolide treatment results in long microtubules since the analogue is less active in the induction of microtubule polymerization compared to discodermolide. Similar results were also shown in our previous study (*29*). Discodermolide analogues with a single change in their chemical structures induce the long microtubules. More interestingly, C19-BPC-discodermolide, although it presents no hypernucleation effect, still displays a strong synergistic effect with Taxol, but not with discodermolide. Therefore, the hypernucleation effect most likely does not play a significant role in either cytotoxicity or synergy with Taxol, and may simply be the manifestation of a remarkable kinetic effect of discodermolide on microtubule assembly.

Discodermolide has synergistic effects with Taxol, the basis of which is not known (*25*). This synergism could be microtubule-based or could result from a nonmicrotubule related interaction. The latter implies that discodermolide may have a unique target other than microtubules in cells. If this were true and related to its synergy with Taxol, we should expect to see synergism between discodermolide and other microtubule stabilizing agents such as epothilone B. However, synergism has not been reported between discodermolide and epothilone B (*25*). Others have suggested that the synergism observed between discodermolide and Taxol could be the result of distinct effects of the two drugs on the microtubule (*51*). In the present study, we demonstrated that C19-BPC-discodermolide also has synergistic effects with Taxol but not with discodermolide, suggesting that C19-BPC-discodermolide acts on microtubules similarly to discodermolide.

In competition experiments, C19-BPC-discodermolide was similar to discodermolide (*17*, *42*) in displacing [^{3}H]Taxol binding to the microtubule, but Taxol could not effectively displace C19-[^{3}H]BPC-discodermolide binding. This may relate to different affinities of the drugs for the microtubule (*42*). It was reported that epothilone B has a higher affinity for microtubules than Taxol (~60-fold compared to Taxol) (*43*), but discodermolide could displace [^{14}C]epothilone B even better than [^{3}H]Taxol (*17*). This indicated that, in addition to different affinities for the microtubule, these drugs may polymerize microtubules with different configurations (*42*). One microtubule configuration induced by a drug could exclude the binding of a second drug. It is known that microtubules polymerized by Taxol have 12 protofilaments, although the preferred number is 13 (*52*). We do not know if microtubules alter their protofilament number when bound to discodermolide. From the competition experiments, both discodermolide and C19-BPC-discodermolide can effectively displace [^{3}H]Taxol. Taxol only partially decreases the binding of C19-[^{3}H]BPC-discodermolide, but discodermolide can effectively displace C19-[^{3}H]BPC-discodermolide. These results suggest that C19-BPC-discodermolide acts on microtubules similarly to discodermolide.

The results from formic acid digestion and immunoprecipitation indicated that C19-BPC- discodermolide binds to amino acid residues 305−445 in β-tubulin. It was reported that discodermolide could reduce tau protein binding to the microtubule (*53*). Since the binding site for tau protein is localized to a peptide in β-tubulin containing amino acid residues 305−445 (*54*), it appears that discodermolide interacts with the same peptide in β-tubulin as does C19-BPC-discodermolide.

Electron crystallographic studies (personal communication, ref *53*) demonstrated that Taxol and discodermolide have overlapping binding sites. This indicated that, like epothilone A (*18*), discodermolide also localizes to the Taxol binding pocket. In the sequence 305−445 in β-tubulin, the only

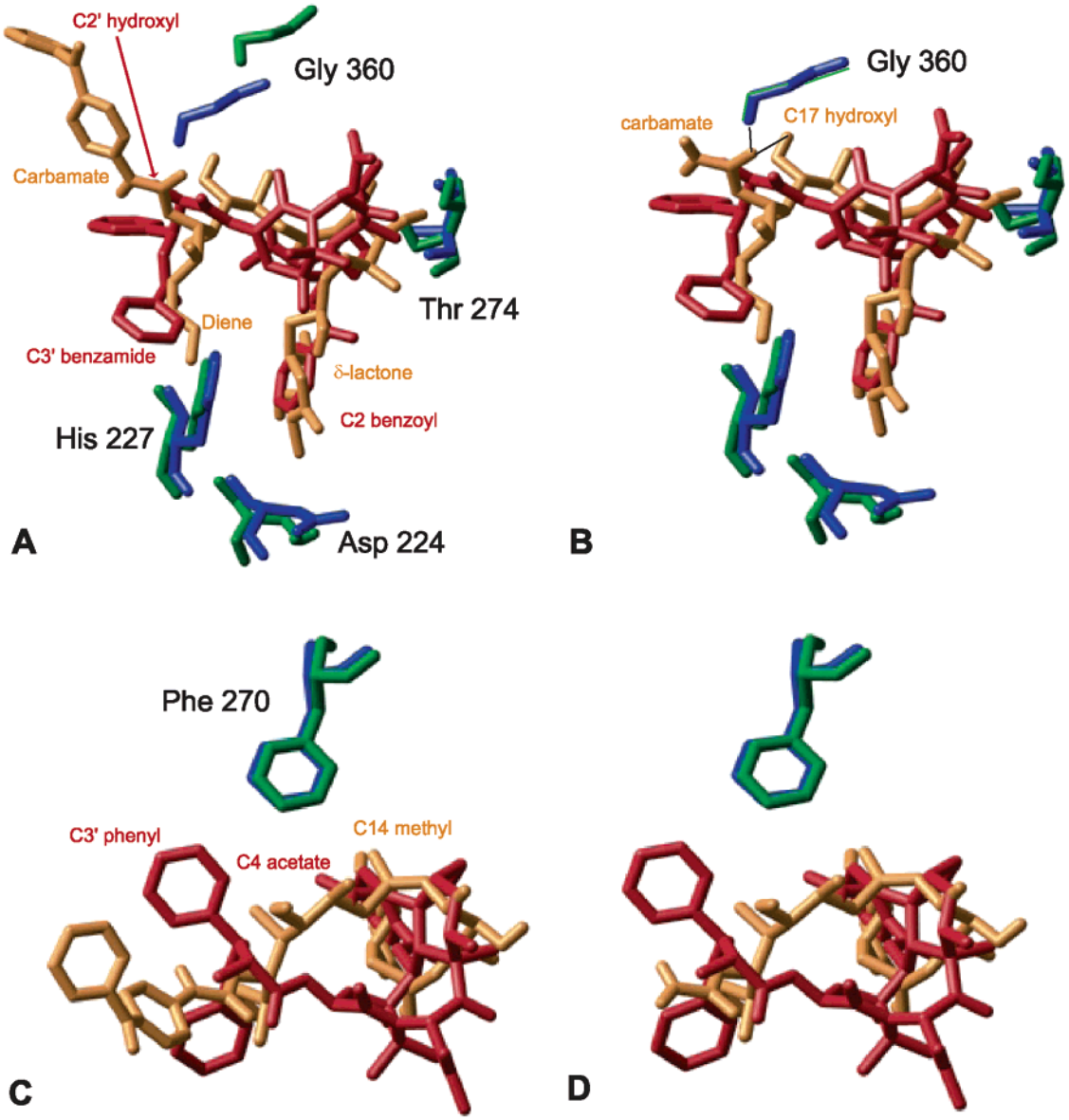

FIGURE 9: Comparisons of the conformation of Taxol to C19-BPC-discodermolide (A and C) and discodermolide (B and D). Viewed from the side (A and B). Viewed from the top (C and D). Taxol is illustrated in red. C19-BPC-discodermolide and discodermolide are shown in orange. The conformation of discodermolide results from the removal of the benzophenone moiety from the C19-BPC-discodermolide model. Green amino acids correspond to the discodermolide/C19-BPC-discodermolide binding model. Blue amino acids correspond to the Taxol/tubulin cocrystal structure. In the C19-BPC-discodermolide binding model, Gly360 is away from the drug because of the conformational change in the S9−S10 loop (A). In the discodermolide binding model, there is no change in the S9−S10 loop and Gly360 is at the same location as that in the Taxol binding model (B). The C19 carbamate O of discodermolide forms hydrogen bonds with its own C17 OH and with the Gly360 NH (B).

region which is close to the Taxol binding pocket is the S9−S10 loop (*6*). This loop contains the five amino acid residues 355−359 identified as labeled by C19-BPC-discodermolide. This also suggests that the discodermolide analogue, C19-BPC-discodermolide, binds to tubulin in a manner similar to that of discodermolide.

In our molecular modeling study on the binding conformation of C19-BPC-discodermolide, the C14 methyl group of C19-BPC-discodermolide is close to Phe 270 in β-tubulin. Shin et al. have suggested that the C14 methyl group of discodermolide makes contact with this amino acid (*55*). In their study, they tested the cytotoxicity of another microtubule stabilizing drug, dictyostatin, and its C16-nor-methyl analogue. They concluded that the C16 methyl of dictyostatin contacts either Phe or Val at position 270. They related dictyostatin to discodermolide since these two drugs have the same relative and absolute stereochemistry (*56*), and proposed that the C14 of discodermolide contacts Phe 270, which is consistent with our data. The hydrophobic interaction between a methyl group and phenylalanine will be maintained when phenylalanine is mutated to another nonpolar hydrophobic amino acid such as valine. Discodermolide retains cytotoxicity to both the parental and mutant cell lines.

From the evidence discussed above, we believe that the discodermolide analogue, C19-BPC-discodermolide, can bind to tubulin in a manner similar to discodermolide. On the basis of the binding conformation of C19-BPC-discodermolide, we have predicted a binding orientation for discodermolide. The discodermolide orientation is derived after the removal of the benzophenone moiety from the C19-BPC-discodermolide, while leaving all other groups intact (Figure 9B,D). In the drug binding pocket in β-tubulin, the δ-lactone of

discodermolide fits into the site in a manner similar to the C2 benzoyl group of Taxol and is close to Asp224. The C19 carbamate of discodermolide extends into another region in this pocket and is close to the S9−S10 loop. This binding orientation of discodermolide is close to our previous proposed discodermolide binding model II (*29*), yet differs in the geometries of two torsional angles at C5−C6 and C18−C19.

The C17 hydroxyl of discodermolide is important for its activity (*30*). We noticed that the C17 hydroxyl is capable of forming a hydrogen bond with the C19 carbamate O without compromising its hydrogen bond to Gly360 (Figure 9B). The resultant conformation disposes the carbamate NH_2 toward the side chain of Asp26 to form a hydrogen bond of 2.6 Å in length. This is similar to the C3′ benzamido NH of Taxol, which forms a hydrogen bond with Asp26 (*6*, *57*). Our model suggests a possible explanation of the role of the C17 hydroxyl in the binding of discodermolide to β-tubulin.

Since discodermolide and C19-BPC-discodermolide have different microtubule polymerization activities, they must interact with microtubule somehow differently. In our model for C19-BPC-discodermolide, the S9−S10 loop has a conformation shift (Figure 8B). The S9−S10 loop is close to the H10 helix. The H10 helix participates in the lateral interactions between two adjacent protofilaments (*6*). C19-BPC-discodermolide causes a shift of the S9−S10 loop. The alteration of the S9−S10 loop may interfere with the H10 helix and the lateral interactions. Discodermolide does not have the benzophenone group and will not cause the shift of the S9−S10 loop.

Similar phenomena were seen when a Taxol photoaffinity analogue, 7-benzophenone Taxol (7-BzDC-Taxol), binds to the microtubule (*5*). 7-BzDC-Taxol can stabilize microtubules formed by GTP but it cannot promote the microtubule polymerization. The benzophenone of 7-BzDC-Taxol photolabels Arg282 in β-tubulin. Arg282 is in the M-loop, which is involved in the lateral interactions between protofilaments (*6*). A bulky benzophenone group of 7-BzDC-Taxol may interfere with the M-loop and thereby modify the lateral interactions, making the function of 7-BzDC-Taxol somehow different from that of Taxol.

The present study suggests that the binding sites for Taxol and discodermolide in the $\alpha\beta$-tubulin dimer are overlapping. Considering the similarities and differences between these two drugs, we suspect that their differences may not be seen in one single tubulin dimer, but rather will be seen in the full length of the microtubule. As suggested previously (*28*, *58*−*60*), Taxol may preferentially bind to the internal core region of the microtubule, whereas discodermolide may bind equally well to the full length of the microtubule. In addition, it has been suggested that Taxol binds weakly to the βIII tubulin isotype (*61*). Discodermolide may also bind differentially to individual tubulin isotypes. In immunofluorescence experiments, microtubule bundles formed in the presence of discodermolide are usually located around the nucleus or at the cell periphery (*12*, *42*). Taxol and discodermolide could preferentially localize to microtubules at different subcellular sites.

In summary, we have evaluated the microtubule stabilizing effects of three photoaffinity analogues of discodermolide, one of which, C19-BPC-discodermolide, was studied in greater detail. It exhibited a synergistic effect with Taxol, but had no hypernucleation effect that was seen only with discodermolide. Photoaffinity labeling studies have suggested that C19-[^{3}H]BPC-discodermolide cross-links the amino acid sequence 305−433, specifically, amino acid residues 355−359 in β-tubulin, which are in proximity to the Taxol binding site. This information enabled us to construct a computationally derived binding model for C19-BPC-discodermolide. We also predicted the orientation of discodermolide in the drug binding pocket.

ACKNOWLEDGMENT

The authors dedicate this manuscript to the memory of our colleague Dr. George A. Orr. They thank Drs. C.-P. H. Yang, H. M. McDaid, and P. Verdier-Pinard for their helpful advice.

REFERENCES

1. Rowinsky, E. K. (1997) The development and clinical utility of the taxane class of antimicrotubule chemotherapy agents, *Annu. Rev. Med. 48*, 353−374.
2. Schiff, P. B., Fant, J., and Horwitz, S. B. (1979) Promotion of microtubule assembly in vitro by taxol, *Nature 277*, 665−667.
3. Rao, S., Krauss, N. E., Heerding, J. M., Swindell, C. S., Ringel, I., Orr, G. A., and Horwitz, S. B. (1994) 3′-(*p*-Azidobenzamido)-taxol photolabels the N-terminal 31 amino acids of beta-tubulin, *J. Biol. Chem. 269*, 3132−3134.
4. Rao, S., Orr, G. A., Chaudhary, A. G., Kingston, D. G., and Horwitz, S. B. (1995) Characterization of the taxol binding site on the microtubule. 2-(m-Azidobenzoyl)taxol photolabels a peptide (amino acids 217−231) of beta-tubulin, *J. Biol. Chem. 270*, 20235−20238.
5. Rao, S., He, L., Chakravarty, S., Ojima, I., Orr, G. A., and Horwitz, S. B. (1999) Characterization of the Taxol binding site on the microtubule. Identification of Arg(282) in beta-tubulin as the site of photoincorporation of a 7-benzophenone analogue of Taxol, *J. Biol. Chem. 274*, 37990−37994.
6. Lowe, J., Li, H., Downing, K. H., and Nogales, E. (2001) Refined structure of alpha beta-tubulin at 3.5 Å resolution, *J. Mol. Biol. 313*, 1045−1057.
7. Li, Y., Poliks, B., Cegelski, L., Poliks, M., Gryczynski, Z., Piszczek, G., Jagtap, P. G., Studelska, D. R., Kingston, D. G., Schaefer, J., and Bane, S. (2000) Conformation of microtubule-bound paclitaxel determined by fluorescence spectroscopy and REDOR NMR, *Biochemistry 39*, 281−291.
8. Ganesh, T., Guza, R. C., Bane, S., Ravindra, R., Shanker, N., Lakdawala, A. S., Snyder, J. P., and Kingston, D. G. (2004) The bioactive Taxol conformation on beta-tubulin: experimental evidence from highly active constrained analogs, *Proc. Natl. Acad. Sci. U.S.A. 101*, 10006−10011.
9. Geney, R., Sun, L., Pera, P., Bernacki, R. J., Xia, S., Horwitz, S. B., Simmerling, C. L., and Ojima, I. (2005) Use of the tubulin bound Paclitaxel conformation for structure-based rational drug design, *Chem. Biol. 12*, 339−348.
10. Orr, G. A., Verdier-Pinard, P., McDaid, H., and Horwitz, S. B. (2003) Mechanisms of Taxol resistance related to microtubules, *Oncogene 22*, 7280−7295.
11. Bollag, D. M., McQueney, P. A., Zhu, J., Hensens, O., Koupal, L., Liesch, J., Goetz, M., Lazarides, E., and Woods, C. M. (1995) Epothilones, a new class of microtubule-stabilizing agents with a taxol-like mechanism of action, *Cancer Res. 55*, 2325−2333.
12. ter Haar, E., Kowalski, R. J., Hamel, E., Lin, C. M., Longley, R. E., Gunasekera, S. P., Rosenkranz, H. S., and Day, B. W. (1996) Discodermolide, a cytotoxic marine agent that stabilizes microtubules more potently than taxol, *Biochemistry 35*, 243−250.
13. Long, B. H., Carboni, J. M., Wasserman, A. J., Cornell, L. A., Casazza, A. M., Jensen, P. R., Lindel, T., Fenical, W., and Fairchild, C. R. (1998) Eleutherobin, a novel cytotoxic agent that induces tubulin polymerization, is similar to paclitaxel (Taxol), *Cancer Res. 58*, 1111−1115.
14. Mooberry, S. L., Tien, G., Hernandez, A. H., Plubrukarn, A., and Davidson, B. S. (1999) Laulimalide and isolaulimalide, new paclitaxel-like microtubule-stabilizing agents, *Cancer Res. 59*, 653−660.

15. Gaitanos, T. N., Buey, R. M., Diaz, J. F., Northcote, P. T., Teesdale-Spittle, P., Andreu, J. M., and Miller, J. H. (2004) Peloruside A does not bind to the taxoid site on beta-tubulin and retains its activity in multidrug-resistant cell lines, *Cancer Res. 64*, 5063−5067.
16. Karjala, G., Chan, Q., Manzo, E., Andersen, R. J., and Roberge, M. (2005) Ceratamines, structurally simple microtubule-stabilizing antimitotic agents with unusual cellular effects, *Cancer Res. 65*, 3040−3043.
17. Madiraju, C., Edler, M. C., Hamel, E., Raccor, B. S., Balachandran, R., Zhu, G., Giuliano, K. A., Vogt, A., Shin, Y., Fournier, J. H., Fukui, Y., Bruckner, A. M., Curran, D. P., and Day, B. W. (2005) Tubulin assembly, taxoid site binding, and cellular effects of the microtubule-stabilizing agent dictyostatin, *Biochemistry 44*, 15053−15063.
18. Nettles, J. H., Li, H., Cornett, B., Krahn, J. M., Snyder, J. P., and Downing, K. H. (2004) The binding mode of epothilone A on alpha, beta-tubulin by electron crystallography, *Science 305*, 866−869.
19. Pineda, O., Farras, J., Maccari, L., Manetti, F., Botta, M., and Vilarrasa, J. (2004) Computational comparison of microtubule-stabilising agents laulimalide and peloruside with taxol and colchicine, *Bioorg. Med. Chem. Lett. 14*, 4825−4829.
20. Longley, R. E., Caddigan, D., Harmody, D., Gunasekera, M., and Gunasekera, S. P. (1991) Discodermolide—a new, marine-derived immunosuppressive compound. I. In vitro studies, *Transplantation 52*, 650−656.
21. Longley, R. E., Caddigan, D., Harmody, D., Gunasekera, M., and Gunasekera, S. P. (1991) Discodermolide—a new, marine-derived immunosuppressive compound. II. In vivo studies, *Transplantation 52*, 656−661.
22. Honore, S., Kamath, K., Braguer, D., Wilson, L., Briand, C., and Jordan, M. A. (2003) Suppression of microtubule dynamics by discodermolide by a novel mechanism is associated with mitotic arrest and inhibition of tumor cell proliferation, *Mol. Cancer Ther. 2*, 1303−1311.
23. Kowalski, R. J., Giannakakou, P., Gunasekera, S. P., Longley, R. E., Day, B. W., and Hamel, E. (1997) The microtubule-stabilizing agent discodermolide competitively inhibits the binding of paclitaxel (Taxol) to tubulin polymers, enhances tubulin nucleation reactions more potently than paclitaxel, and inhibits the growth of paclitaxel-resistant cells, *Mol. Pharmacol. 52*, 613−622.
24. He, L., Yang, C. P., and Horwitz, S. B. (2001) Mutations in beta-tubulin map to domains involved in regulation of microtubule stability in epothilone-resistant cell lines, *Mol. Cancer Ther. 1*, 3−10.
25. Martello, L. A., McDaid, H. M., Regl, D. L., Yang, C. P., Meng, D., Pettus, T. R., Kaufman, M. D., Arimoto, H., Danishefsky, S. J., Smith, A. B., III, and Horwitz, S. B. (2000) Taxol and discodermolide represent a synergistic drug combination in human carcinoma cell lines, *Clin. Cancer Res. 6*, 1978−1987.
26. Klein, L. E., Freeze, B. S., Smith, A. B., III, and Horwitz, S. B. (2005) The microtubule stabilizing agent discodermolide is a potent inducer of accelerated cell senescence, *Cell Cycle 4*, 501−507.
27. Huang, G. S., Lopez-Barcons, L., Freeze, B. S., Smith, A. B., III, Goldberg, G. L., Horwitz, S. B., and McDaid, H. M. (2006) Potentiation of taxol efficacy by discodermolide in ovarian carcinoma xenograft-bearing mice, *Clin. Cancer Res. 12*, 298−304.
28. Honore, S., Kamath, K., Braguer, D., Horwitz, S. B., Wilson, L., Briand, C., and Jordan, M. A. (2004) Synergistic suppression of microtubule dynamics by discodermolide and paclitaxel in non-small cell lung carcinoma cells, *Cancer Res. 64*, 4957−4964.
29. Martello, L. A., LaMarche, M. J., He, L., Beauchamp, T. J., Smith, A. B., and Horwitz, S. B. (2001) The relationship between Taxol and (+)-discodermolide: synthetic analogs and modeling studies, *Chem. Biol. 8*, 843−855.
30. Gunasekera, S. P., Longley, R. E., and Isbrucker, R. A. (2002) Semisynthetic analogues of the microtubule-stabilizing agent discodermolide: preparation and biological activity, *J. Nat. Prod. 65*, 1830−1837.
31. Minguez, J. M., Kim, S. Y., Giuliano, K. A., Balachandran, R., Madiraju, C., Day, B. W., and Curran, D. P. (2003) Synthesis and biological assessment of simplified analogues of the potent microtubule stabilizer (+)-discodermolide, *Bioorg. Med. Chem. 11*, 3335−3357.
32. Smith, A. B., III, Freeze, B. S., Lamarche, M. J., Hirose, T., Brouard, I., Rucker, P. V., Xian, M., Sundermann, K. F., Shaw, S. J., Burlingame, M. A., Horwitz, S. B., and Myles, D. C. (2005) Design, synthesis, and evaluation of carbamate-substituted analogues of (+)-discodermolide, *Org. Lett. 7*, 311−314.
33. Smith, A. B., III, Rucker, P. V., Brouard, I., Freeze, B. S., Xia, S., and Horwitz, S. B. (2005) Design, synthesis, and biological evaluation of potent discodermolide fluorescent and photoaffinity molecular probes, *Org. Lett. 7*, 5199−5202.
34. Parness, J., and Horwitz, S. B. (1981) Taxol binds to polymerized tubulin in vitro, *J. Cell Biol. 91*, 479−487.
35. Diaz, J. F., and Andreu, J. M. (1993) Assembly of purified GDP-tubulin into microtubules induced by taxol and taxotere: reversibility, ligand stoichiometry, and competition, *Biochemistry 32*, 2747−2755.
36. Zhou, R. P., Oskarsson, M., Paules, R. S., Schulz, N., Cleveland, D., and Vande Woude, G. F. (1991) Ability of the c-mos product to associate with and phosphorylate tubulin, *Science 251*, 671−675.
37. Wu, Q., Bounaud, P. Y., Kuduk, S. D., Yang, C. P., Ojima, I., Horwitz, S. B., and Orr, G. A. (1998) Identification of the domains of photoincorporation of the 3′- and 7-benzophenone analogues of taxol in the carboxyl-terminal half of murine mdr1b P-glycoprotein, *Biochemistry 37*, 11272−11279.
38. Rai, S. S., and Wolff, J. (1996) Localization of the vinblastine-binding site on beta-tubulin, *J. Biol. Chem. 271*, 14707−14711.
39. Olmsted, J. B., and Borisy, G. G. (1973) Characterization of microtubule assembly in porcine brain extracts by viscometry, *Biochemistry 12*, 4282−4289.
40. Choy, N., Shin, Y., Nguyen, P. Q., Curran, D. P., Balachandran, R., Madiraju, C., and Day, B. W. (2003) Simplified discodermolide analogues: synthesis and biological evaluation of 4-*epi*-7-dehydroxy-14,16-didemethyl-(+)-discodermolides as microtubule-stabilizing agents, *J. Med. Chem. 46*, 2846−2864.
41. Smith, A. B., III, Freeze, B. S., Lamarche, M. J., Hirose, T., Brouard, I., Xian, M., Sundermann, K. F., Shaw, S. J., Burlingame, M. A., Horwitz, S. B., and Myles, D. C. (2005) Design, synthesis, and evaluation of analogues of (+)-14-normethyldiscodermolide, *Org. Lett. 7*, 315−318.
42. Hung, D. T., Chen, J., and Schreiber, S. L. (1996) (+)-Discodermolide binds to microtubules in stoichiometric ratio to tubulin dimers, blocks taxol binding and results in mitotic arrest, *Chem. Biol. 3*, 287−293.
43. Buey, R. M., Barasoain, I., Jackson, E., Meyer, A., Giannakakou, P., Paterson, I., Mooberry, S., Andreu, J. M., and Diaz, J. F. (2005) Microtubule interactions with chemically diverse stabilizing agents: thermodynamics of binding to the paclitaxel site predicts cytotoxicity, *Chem. Biol. 12*, 1269−1279.
44. Breitling, F., and Little, M. (1986) Carboxy-terminal regions on the surface of tubulin and microtubules. Epitope locations of YOL1/34, DM1A and DM1B, *J. Mol. Biol. 189*, 367−370.
45. Audebert, S., White, D., Cosson, J., Huitorel, P., Edde, B., and Gagnon, C. (1999) The carboxy-terminal sequence Asp427-Glu432 of beta-tubulin plays an important function in axonemal motility, *Eur. J. Biochem. 261*, 48−56.
46. Nunes, M., Kaplan, J., Wooters, J., Hari, M., Minnick, A. A., Jr., May, M. K., Shi, C., Musto, S., Beyer, C., Krishnamurthy, G., Qiu, Y., Loganzo, F., Ayral-Kaloustian, S., Zask, A., and Greenberger, L. M. (2005) Two photoaffinity analogues of the tripeptide, hemiasterlin, exclusively label alpha-tubulin, *Biochemistry 44*, 6844−6857.
47. Snyder, J. P., Nettles, J. H., Cornett, B., Downing, K. H., and Nogales, E. (2001) The binding conformation of Taxol in beta-tubulin: a model based on electron crystallographic density, *Proc. Natl. Acad. Sci. U.S.A. 98*, 5312−5316.
48. Kawakami, K., Oda, N., Miyoshi, K., Funaki, T., and Ida, Y. (2006) Solubilization behavior of a poorly soluble drug under combined use of surfactants and cosolvents, *Eur. J. Pharm. Sci. 28*, 7−14.
49. Isbrucker, R. A., Gunasekera, S. P., and Longley, R. E. (2001) Structure-activity relationship studies of discodermolide and its semisynthetic acetylated analogs on microtubule function and cytotoxicity, *Caner Chemother. Pharmacol. 48*, 29−36.
50. Kowalski, R. J., Giannakakou, P., and Hamel, E. (1997) Activities of the microtubule-stabilizing agents epothilones A and B with purified tubulin and in cells resistant to paclitaxel (Taxol(R)), *J. Biol. Chem. 272*, 2534−2541.
51. Giannakakou, P., and Fojo, T. (2000) Discodermolide: just another microtubule-stabilizing agent? No! A lesson in synergy, *Clin. Cancer Res. 6*, 1613−1615.

52. Diaz, J. F., Valpuesta, J. M., Chacon, P., Diakun, G., and Andreu, J. M. (1998) Changes in microtubule protofilament number induced by Taxol binding to an easily accessible site. Internal microtubule dynamics, *J. Biol. Chem. 273*, 33803−33810.
53. Kar, S., Florence, G. J., Paterson, I., and Amos, L. A. (2003) Discodermolide interferes with the binding of tau protein to microtubules, *FEBS Lett. 539*, 34−36.
54. Chau, M. F., Radeke, M. J., de Ines, C., Barasoain, I., Kohlstaedt, L. A., and Feinstein, S. C. (1998) The microtubule-associated protein tau cross-links to two distinct sites on each α and β tubulin monomer via separate domains, *Biochemistry 37*, 17692−17703.
55. Shin, Y., Fournier, J. H., Balachandran, R., Madiraju, C., Raccor, B. S., Zhu, G., Edler, M. C., Hamel, E., Day, B. W., and Curran, D. P. (2005) Synthesis and biological evaluation of (−)-16-normethyldictyostatin: a potent analogue of (−)-dictyostatin, *Org. Lett. 7*, 2873−2876.
56. Shin, Y., Fournier, J. H., Fukui, Y., Bruckner, A. M., and Curran, D. P. (2004) Total synthesis of (−)-dictyostatin: confirmation of relative and absolute configurations, *Angew. Chem. Int. Ed. 43*, 4634−4637.
57. Hari, M., Loganzo, F., Annable, T., Tan, X., Musto, S., Morilla, D. B., Nettles, J. H., Snyder, J. P., and Greenberger, L. M. (2006) Paclitaxel-resistant cells have a mutation in the paclitaxel-binding region of {beta}-tubulin (Asp26Glu) and less stable microtubules, *Mol. Cancer Ther. 5*, 270−278.
58. Carlier, M. F., and Pantaloni, D. (1983) Taxol effect on tubulin polymerization and associated guanosine 5′-triphosphate hydrolysis, *Biochemistry 22*, 4814−4822.
59. Derry, W. B., Wilson, L., and Jordan, M. A. (1995) Substoichiometric binding of taxol suppresses microtubule dynamics, *Biochemistry 34*, 2203−2211.
60. Panda, D., Miller, H. P., and Wilson, L. (2002) Determination of the size and chemical nature of the stabilizing "cap" at microtubule ends using modulators of polymerization dynamics, *Biochemistry 41*, 1609−1617.
61. Ferlini, C., Raspaglio, G., Mozzetti, S., Cicchillitti, L., Filippetti, F., Gallo, D., Fattorusso, C., Campiani, G., and Scambia, G. (2005) The seco-taxane IDN5390 is able to target class III beta-tubulin and to overcome paclitaxel resistance, *Cancer Res. 65*, 2397−2405.

BI060497A